Intermetallics 55 (2014) 123–128

Contents lists available at ScienceDirect

Intermetallics

journal homepage: www.elsevier.com/locate/intermet

Structural transformations in $R_3Cu_4Sn_4$ (R = Ho, Er, Tm) intermetallic compounds

J.M. Cadogan [a, *], S. Muñoz Pérez [a], R. Cobas [a], D.H. Ryan [b], R. Lora-Serrano [c], M.J.S. Figueira [c], F. Yokaichiya [d]

[a] School of Physical, Environmental and Mathematical Sciences, UNSW Canberra at the Australian Defence Force Academy, Canberra, ACT, BC 2610, Australia
[b] Department of Physics, McGill University, Montreal, Québec, H3A 2T8, Canada
[c] Instituto de Física, Universidade Federal de Uberlândia, 38400-902, Uberlândia, MG, Brazil
[d] Laboratório Nacional de Luz Síncrotron, Campinas, SP, Brazil

ARTICLE INFO

Article history:
Received 30 June 2014
Received in revised form
23 July 2014
Accepted 24 July 2014
Available online

Keywords:
A. Rare-earth intermetallics
B. Phase transformation
B. Crystal chemistry
F. Diffraction/scaterring

ABSTRACT

The family of ternary intermetallic compounds $R_3T_4X_4$ (R = rare-earth; T = d-element; X = Si, Ge, Sn) comprises over 100 members that have a generic orthorhombic structure (space group *Immm*, #71) at room temperature. We have observed a monoclinic ↔ orthorhombic crystallographic transformation in $Ho_3Cu_4Sn_4$, $Er_3Cu_4Sn_4$ and $Tm_3Cu_4Sn_4$ by high-resolution synchrotron X-ray and neutron powder diffraction. We show that the temperature at which this transformation occurs scales linearly with the ionic radius of the rare-earth. No such transformation was observed in $Dy_3Cu_4Sn_4$, down to 1.7 K, consistent with this scaling.

1. Introduction

The $R_3T_4X_4$ family (R = rare earth; T = Cu, Ag, Au, Pd, Mn; X = Si, Ge, Sn) is an extensive series of isostructural intermetallic compounds that exhibit a rich variety of magnetic ordering. The intrinsic magnetic behaviour of this family of compounds has been the subject of numerous studies by neutron diffraction, magnetometry and Mössbauer spectroscopy. The R atoms occupy two distinct crystallographic sites in the orthorhombic unit cell and, in general, the R moments order antiferromagnetically, with distinct magnetic structures being adopted by the two R sublattices. In many cases, the two R sites have quite different ordering temperatures and we refer the reader to our recent review of the magnetism of the $R_3T_4X_4$ compounds [1] for a detailed discussion of this system. A useful summary of the magnetic properties of the $R_3T_4X_4$ compounds has also been written by Wawrzyńska and Szytuła [2].

At room temperature (RT), the $R_3T_4X_4$ compounds have a generic orthorhombic $Gd_3Cu_4Ge_4$-type structure (space group *Immm*, #71) [3,4] with two formula units per orthorhombic cell. The R atoms occupy two crystallographic sites (2*a* and 4*f*), the transition metal (T) occupies the 8*m* site and the X atoms occupy the 4*e* and 4*j* sites. The exceptions to this orthorhombic structure are $Tm_3Cu_4Sn_4$ [4] and $Lu_3Cu_4Sn_4$ [5] which have a monoclinic *C2/m* structure (or *I2/m* in a different setting of the Space Group #12) at RT. In a recent paper [6] we showed that $Tm_3Cu_4Sn_4$ transforms from the monoclinic *I2/m* structure to the generic orthorhombic *Immm* structure when heated above RT and we determined the transition temperature to be 458(3) K by X-ray diffraction. In a previous brief report we noted that $Er_3Cu_4Sn_4$ and $Ho_3Cu_4Sn_4$ present similar phase transitions at different temperatures [7].

In this paper we will focus on the crystallography of the $R_3Cu_4Sn_4$ members of this extensive family. Magnetic and crystallographic studies of the $R_3Cu_4Sn_4$ compounds encompass virtually the entire rare-earth series: R = La [8], Ce [9,10], Pr [8,11,12], Nd [8,11–13], Sm [8], Gd [9,14–18], Tb [14,15,19,20], Dy [14,15,19,7], Ho [13–15,19,20,22–24,7], Er [14,15,19,25,26,7], Tm [4,6,21] and Lu [5].

During the course of our neutron diffraction work on the $Er_3Cu_4X_4$ (X = Si, Ge, Sn) compounds [25], we observed significant broadening of the nuclear peaks when X = Sn at temperatures around 200–250 K, well above the magnetic ordering temperatures of the two Er sublattices, namely 6 K and 3.5 K [19]. Upon cooling below 200 K, many of these broadened peaks split, suggesting a crystallographic distortion to a symmetry lower than the generic *Immm* orthorhombic symmetry.

Here, we present the results of our high-resolution synchrotron radiation and neutron powder diffraction measurements made on

* Corresponding author.
E-mail address: s.cadogan@adfa.edu.au (J.M. Cadogan).

http://dx.doi.org/10.1016/j.intermet.2014.07.016
0966-9795/

$Dy_3Cu_4Sn_4$, $Ho_3Cu_4Sn_4$ and $Er_3Cu_4Sn_4$ and $Tm_3Cu_4Sn_4$. The monoclinic to orthorhombic phase transition that occurs when R = Ho, Er and Tm is discussed. The crystallographic transition temperature scales linearly with the ionic radius of the rare-earth. There is no such distortion in $Dy_3Cu_4Sn_4$ down to 1.7 K, in agreement with the scaling law.

2. Experimental methods

Stoichiometric amounts of the pure elements (R 99.9 wt.%, Cu and Sn 99.999 wt.%) were arc-melted under high-purity argon. The resulting ingots were then sealed under vacuum in quartz tubes and annealed for 20 days at 873 K, followed by water quenching. Cu-K_α X-ray diffraction and electron microprobe analyses, carried out at RT, confirmed that the majority phase was the orthorhombic *Immm* phase for R = Dy, Ho and Er, whereas the RT structure of $Tm_3Cu_4Sn_4$ is monoclinic *C2/m* (*I2/m*), in agreement with Thirion et al. [4]. Despite numerous attempts, we were unable to avoid the production of small amounts (less than 3 wt%) of the respective hexagonal RCuSn phases.

High-resolution Synchrotron X-ray Diffraction (SXRD) was carried out at the XPD beamline of the LNLS facility in Campinas, Brazil, using a wavelength (λ) of 1.23984(2) Å. Neutron diffraction (ND) experiments were carried out on the *C2* multi-wire powder diffractometer (DUALSPEC) at the NRU reactor, Canadian Neutron Beam Centre, Chalk River, Ontario. The neutron wavelengths were 2.3721(2) Å and 1.3306(2) Å, using both position settings of the DUALSPEC diffractometer, which allowed us to cover a *Q* range from 0.23 $Å^{-1}$ to 7.96 $Å^{-1}$. All refinements of the SXRD and ND patterns employed FullProf/WinPlotr [27,28].

3. Results and discussion

In this section we will present the results of our diffraction experiments, placing the emphasis on $Er_3Cu_4Sn_4$. Following the detailed discussion of $Er_3Cu_4Sn_4$ we will briefly present our results on $Ho_3Cu_4Sn_4$ and $Tm_3Cu_4Sn_4$, obtained using the same procedure as for $Er_3Cu_4Sn_4$. Finally, we will present our diffraction results on $Dy_3Cu_4Sn_4$ in which we see no evidence for a distortion, down to 1.7 K. We will show that this behaviour is consistent with the dependence of the crystallographic distortion on the ionic radius of the rare-earth.

For the purposes of comparison with the orthorhombic *Immm* cell, we will present our monoclinic refinements within the *I2/m* 'unique *b*-axis' setting of space group #12. Transformations between the various settings within a monoclinic space group can be accomplished using the freely available programs *SETSTRU* on the Bilbao Crystallographic Web Server [29], VESTA [30] and PowderCell [31].

3.1. Crystal structure of $Er_3Cu_4Sn_4$

In Fig. 1 we show the refinements of the SXRD patterns of $Er_3Cu_4Sn_4$ obtained at 298 K and 1.7 K. The effects of the orthorhombic → monoclinic transformation upon cooling is clear, particularly with the splitting of the single (411) orthorhombic peak into the two monoclinic peaks $(\bar{4}11)$ and (411) at $2\theta \sim 24.7°$ (*I2/m* with $a > c > b$). These monoclinic peaks in the alternate *C2/m* space group setting are $(\bar{5}11)$ and (311).

In Fig. 2 we show the refinements of the ND patterns obtained at 298 K using the two position settings of the DUALPSEC diffractometer. Co-refinement of the SXRD and ND patterns of $Er_3Cu_4Sn_4$ obtained at 298 K confirm the formation of the generic orthorhombic $Gd_3Cu_4Ge_4$-type structure. The refined lattice parameters are in excellent agreement with the work of Thirion et al. [4] and Wawrzyńska et al. [11]. In Table 1 we give the atomic positional parameters of $Er_3Cu_4Sn_4$ obtained by the simultaneous refinement of the diffraction patterns.

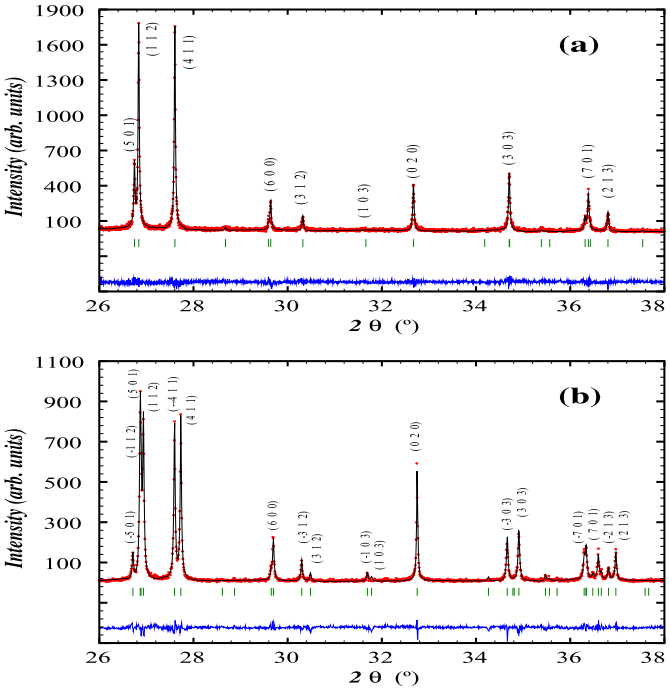

Fig. 1. Refined SXRD patterns of $Er_3Cu_4Sn_4$, obtained at (a) 298 K and (b) 1.7 K, with λ = 1.23984(2)Å. The Bragg markers represent the scattering from the $Er_3Cu_4Sn_4$ crystal structure (orthorhombic *Immm* at 298 K and monoclinic *I2/m* (*C2/m*) at 1.7 K).

3.1.1. Crystallographic transformation

Upon cooling from room temperature we noticed a broadening of the peaks in the ND patterns of $Er_3Cu_4Sn_4$ at around 260 K. This

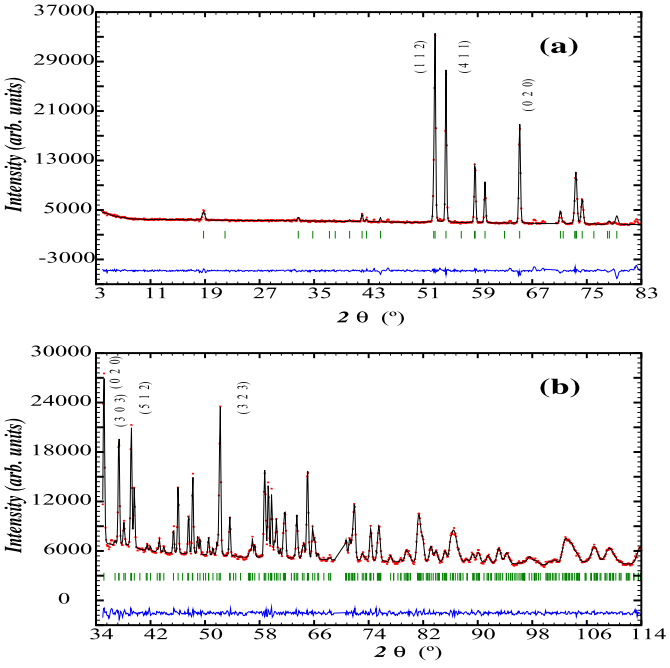

Fig. 2. Refined ND patterns of $Er_3Cu_4Sn_4$, obtained at 298 K. The Bragg markers represent the scattering from the orthorhombic *Immm* crystal structure. (a) λ = 2.3721(2) Å and (b) λ = 1.3306(2) Å.

Table 1
Crystallographic data for $Er_3Cu_4Sn_4$ obtained by refinement of the SXRD and ND patterns.

T = 298 K Orthorhombic *Immm*			T = 1.7 K Monoclinic *I2/m*		
Atom	Site	Coordinates	Atom	Site	Coordinates
Er	2*a*	0, 0, 0	Er	2*a*	0, 0, 0
Er	4*f*	0.3680(4), 1/2, 0	Er	4*i*	0.8694(5), 0, 0.5092(10)
Cu	8*m*	0.3268(6), 0, 0.31320(10)	Cu	4*i*	0.6628(11), 0, 0.6836(24)
			Cu	4*i*	0.6789(12), 0, 0.3107(23)
Sn	4*e*	0.2161(6), 0, 0	Sn	4*i*	0.7811(7), 0, 0.9914(15)
Sn	4*j*	1/2, 0, 0.2022(9)	Sn	4*i*	0.4931(7), 0, 0.7963(14)
	a (Å)	14.5455(5)			14.5003(5)
	b (Å)	4.4088(2)			4.3929(2)
	c (Å)	6.9043(2)			6.8810(2)
	β (°)	90			90.48(1)
	R (F)	13.8			13.2
	R (Bragg)	16.9			18.0

was followed by a splitting of the peaks upon further cooling below 250 K, substantially higher than the magnetic ordering temperatures of the two Er sublattices (6 K and 3.5 K [19]). To investigate the possibility that $Er_3Cu_4Sn_4$ might undergo a symmetry-lowering crystallographic distortion below room temperature, we obtained a set of ND patterns over the temperature range 3.8 K–300 K. In Fig. 3 we show the temperature dependence of the diffraction pattern region around $2\theta \sim 55°$ (with $\lambda = 2.3721(2)$ Å).

The splitting of the orthorhombic (411) peak at $2\theta = 55°$ is prominent and we can rule out a magnetic cause for it since the broadening/splitting upon cooling clearly has begun by 200 K, substantially higher than the magnetic ordering transition of the Er(2d) sublattice at 6 K.

To characterise more fully the crystallographic distortion we carried out high-resolution X-ray diffraction (SXRD) at the LNLS facility. Fig. 4 shows a series of SXRD diffraction patterns, once again showing the broadening/splitting of the orthorhombic peaks as a function of temperature, as the symmetry lowers. In particular, we concentrate on the temperature evolution of the $(\bar{4}11)$ and (411) monoclinic peaks as they merge to form the (411) orthorhombic peak.

The vast majority of the $R_3T_4X_4$ compounds form in the orthorhombic *Immm* cell but the crystal structures of $Tm_3Cu_4Sn_4$ and

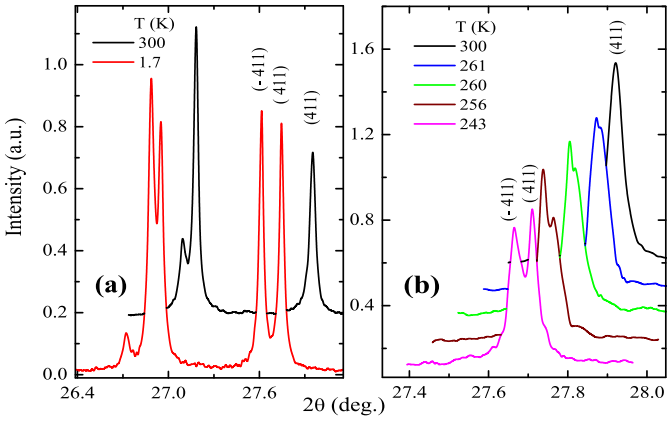

Fig. 4. Sections of the SXRD patterns of $Er_3Cu_4Sn_4$, obtained over the temperature range 1.7–300 K. The two peaks in the orthorhombic phase (300 K) are the overlapping (501)/(112) (lower angle) and the (411) (higher angle) peaks. In (b) we focus on the temperature evolution of the (411) peak. The patterns have been offset both horizontally and vertically with respect to each other for clarity. ($\lambda = 1.23984(2)$ Å).

$Lu_3Cu_4Sn_4$ were reported to be monoclinic *C2/m* (#12) at room temperature [4,5]. The *b* and *c* lattice parameters are identical to those of the 'parent' orthorhombic cell but the *a* parameter is about 10% larger. Of most significance is the rather large value of the angle *β*. There are a number of possible crystallographic descriptions for monoclinic cells and the monoclinic *C2/m* cell can be transformed to a body-centred cell with a *β* angle much closer to 90°. We transformed the *C2/m* cell of $Tm_3Cu_4Sn_4$ to the body-centred *I2/m* (#12) form which is closely related to the parent orthorhombic *Immm* cell (see Fig. 9), showing the limited extent of the structural distortion. The transformed lattice parameters and atomic positions in this body-centred cell are given in Table 1. In Fig. 5 we show the temperature dependencies of the angular positions of the $(\bar{4}11)$ and (411) monoclinic peaks. At temperatures above the transition temperature, these peaks give way to the orthorhombic (411) peak. These data indicate the completion of the transformation to the orthorhombic structure at 262(2) K.

The relationship between the monoclinic (*C2/m* and *I2/m*) and orthorhombic (*Immm*) forms of $Er_3Cu_4Sn_4$ is shown in our paper on $Tm_3Cu_4Sn_4$ [6]. As discussed there, the most significant difference is

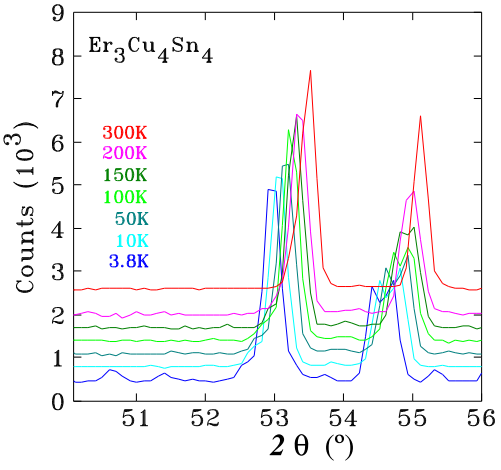

Fig. 3. Sections of the ND patterns of $Er_3Cu_4Sn_4$, obtained over the temperature range 3.8–300 K. The two peaks in the orthorhombic phase (300 K) are the overlapping (501)/(112) (lower angle) and the (411) (higher angle) peaks, respectively. The patterns have been offset both horizontally and vertically with respect to each other for clarity. ($\lambda = 2.3721(2)$ Å).

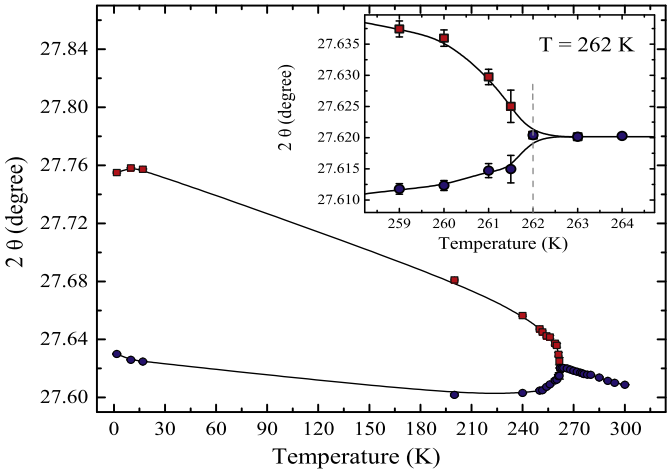

Fig. 5. Temperature dependencies of the (−411) (blue–lower) and (411) (red–upper) monoclinic peak positions of $Er_3Cu_4Sn_4$, based on refinement of the SXRD patterns. (For interpretation of the references to colour in this figure legend, the reader is referred to the web version of this article.)

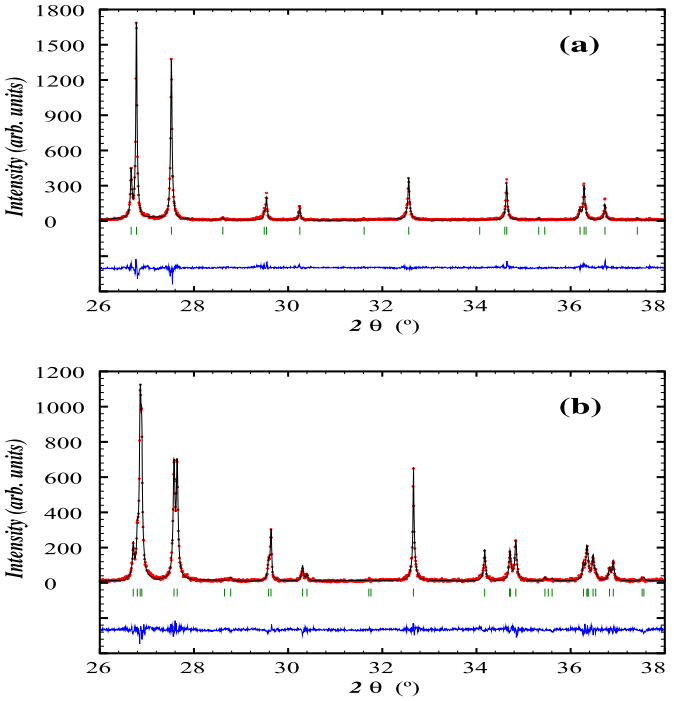

Fig. 6. Refined SXRD patterns of $Ho_3Cu_4Sn_4$, obtained at 298 K (a) and 1.7 K (b). The Bragg markers represent the scattering from the orthorhombic *Immm* structure at 298 K and the monoclinic *I2/m* structure at 1.7 K. The patterns were obtained with $\lambda = 1.23984(2)$ Å.

in the atomic positions of the Cu(2) sites whose relative displacement is nearly three times those of the other sites. In the orthorhombic *Immm* structure, the Cu atoms occupy a single crystallographic site (8*m*) with the point group *m*. As a consequence of the transformation to the monoclinic cell, the Cu orthorhombic *8m* site splits into two 4*i* sites. Finally, the fact that only the Tm and Lu copper-stannides have the monoclinic phase at room temperature suggested that the size of the R ion might play a major role in determining the crystallography in the $R_3Cu_4Sn_4$ intermetallic series (*vide infra*).

3.2. Crystal structure of $Ho_3Cu_4Sn_4$

In Fig. 6(a) we show the refinement of the SXRD pattern of $Ho_3Cu_4Sn_4$ obtained at 298 K. The SXRD and ND patterns of $Ho_3Cu_4Sn_4$ obtained at 298 K confirm the formation of the generic

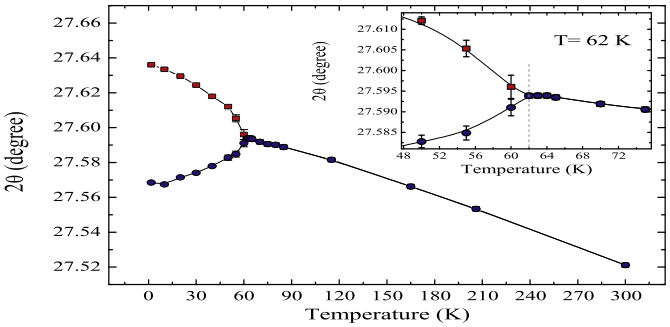

Fig. 7. Temperature dependencies of the (−411) (blue−lower) and (411) (red−upper) monoclinic peak positions of $Ho_3Cu_4Sn_4$, based on refinement of the SXRD patterns. (For interpretation of the references to colour in this figure legend, the reader is referred to the web version of this article.)

orthorhombic structure. The refined lattice parameters at 298 K are given in Table 2 and are in good agreement with data reported in references [4,11]. The refined atomic position parameters of $Ho_3Cu_4Sn_4$, deduced from the refinement of the SXRD data, are given in Table 2.

3.2.1. Crystallographic distortion

Fig. 6(b) shows the SXRD pattern of $Ho_3Cu_4Sn_4$, obtained at 1.7 K and refined in terms of the monoclinic *I2/m* group. The structural transformation from the RT orthorhombic phase to the low-T monoclinic phase is clearly seen as the monoclinic peaks emerge from the splitting of the higher-symmetry orthorhombic peaks. In Fig. 7 we show the angular positions of the $(\bar{4}11)$ and (411) monoclinic peaks as they emerge from the (411) orthorhombic peak, as a function of temperature. These data show the transformation to the orthorhombic structure occurring at 62(2) K.

3.3. Crystal structure of $Tm_3Cu_4Sn_4$

We have already reported the results of our high-temperature X-ray diffraction study of $Tm_3Cu_4Sn_4$ in a previous paper [6] so here we will simply summarize the main findings of that study. At room temperature, the crystal structure of $Tm_3Cu_4Sn_4$ is monoclinic *C2/m*–*I2/m* [4,6,21] with the refined lattice parameters at 295 K given in Table 3. Upon heating above room temperature we observed several of the monoclinic diffraction peaks merge, indicating a transition to a higher symmetry. We followed the crystallographic transformation by monitoring the peak width upon heating and we also observed the transition by Differential

Table 2
Crystallographic data for $Ho_3Cu_4Sn_4$ obtained by refinement of the SXRD diffraction patterns.

T = 298 K Orthorhombic *Immm*			*T* = 1.7 K Monoclinic *I2/m*		
Atom	Site	Coordinates	Atom	Site	Coordinates
Ho	2*a*	0, 0, 0	Ho	2*a*	0, 0, 0
Ho	4*f*	0.3691(4), 1/2, 0	Ho	4*i*	0.8695(3), 0, 0.5038(7)
Cu	8*m*	0.3283(7), 0, 0.3110(14)	Cu	4*i*	0.6679(7), 0, 0.6879(16)
			Cu	4*i*	0.6768(7), 0, 0.3081(15)
Sn	4*e*	0.2161(5),0, 0	Sn	4*i*	0.7848(4), 0, 0.9913(10)
Sn	4*j*	1/2, 0, 0.2023(12)	Sn	4*i*	0.4970(5), 0, 0.7992(8)
	a (Å)	14.5893(5)			14.5445(3)
	b (Å)	4.4227(1)			4.4096(1)
	c (Å)	6.9121(2)			6.8863(1)
	β(°)	90			90.26(1)
	R (F)	14.5			8.8
	R (Bragg)	16.6			13.2

Table 3
Crystallographic data for $Tm_3Cu_4Sn_4$.

T = 295 K Monoclinic *I2/m*			*T* = 485 K Orthorhombic *Immm*		
Atom	Site	Coordinates	Atom	Site	Coordinates
Tm	2*a*	0, 0, 0	Tm	2*a*	0, 0, 0
Tm	4*i*	0.8702(1), 0, 0.5075(4)	Tm	4*f*	0.3718(2), 1/2, 0
Cu	4*i*	0.6642(3), 0, 0.6875(7)	Cu	8*m*	0.3249(2), 0, 0.3149(5)
Cu	4*i*	0.6791(4), 0, 0.3088(7)			
Sn	4*i*	0.7843(2), 0, 0.9899(5)	Sn	4*e*	0.2175(2), 0, 0
Sn	4*i*	0.4944(2), 0, 0.7941(4)	Sn	4*j*	1/2, 0, 0.2018(3)
	a (Å)	14.4911(3)			14.5261(4)
	b (Å)	4.3898(1)			4.4028(1)
	c (Å)	6.8931(1)			6.9139(2)
	β (°)	90.54(1)			90
	R (profile)	2.0			3.4
	R (Bragg)	1.2			1.2

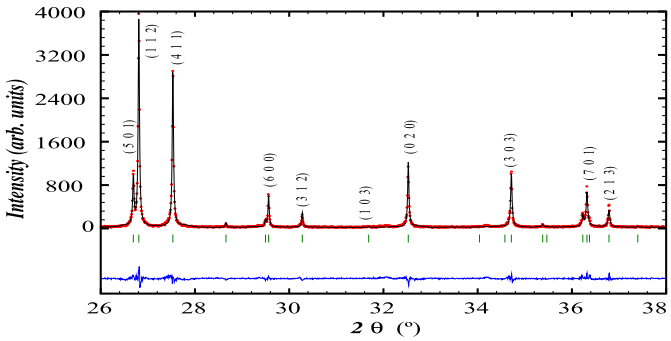

Fig. 8. Refined SXRD pattern of $Dy_3Cu_4Sn_4$, obtained at 1.7 K. The Bragg markers represent the orthorhombic *Immm* crystal structure. $\lambda = 1.23984(2)$ Å.

Scanning Calorimetry. The transformation temperature in $Tm_3Cu_4Sn_4$ is 458(3) K.

3.4. Crystal structure of $Dy_3Cu_4Sn_4$

In Fig. 8 we show the SXRD pattern of $Dy_3Cu_4Sn_4$ obtained at 1.7 K. Refinement of this pattern indicates that $Dy_3Cu_4Sn_4$ retains the orthorhombic *Immm* structure down to 1.7 K. We see no evidence of the peak splitting seen in the other compounds. In Table 4 we give the refined atomic position parameters of $Dy_3Cu_4Sn_4$, deduced from the refinement of our SXRD pattern.

4. Discussion

As discussed in detail previously [6], the most significant difference between the orthorhombic and monoclinic crystal structures of the $R_3Cu_4Sn_4$ stannides lies with the Cu sites, whose relative atomic displacement parameters are nearly three times those of the other atoms, as obtained from the Rietveld refinements. The distortion may also be seen in the tilting of the Sn–Sn pairs relative to the R–R axes. In Fig. 9 we compare the monoclinic and orthorhombic cells of the $R_3Cu_4Sn_4$ compounds. These figures were drawn using the VESTA software [30] and emphasise the limited extent of the crystallographic transformation from the orthorhombic *Immm* cell to the monoclinic *I2/m* cell.

In Fig. 10 we show the dependence of the structural transformation temperature on the ionic radius of the rare-earth. The values for the ionic radii were taken from Ref. [32] and reflect 6-, 8- and 9-fold coordination. The transition temperatures marking the monoclinic ↔ orthorhombic transformation in $R_3Cu_4Sn_4$ for R = Ho, Er and Tm scale linearly with the ionic radius. It is also clear from the fact that the extrapolated transformation temperature for $Dy_3Cu_4Sn_4$ lies well below $T = 0$ that no such transformation would be expected in $Dy_3Cu_4Sn_4$, in keeping with our experimental observations (down to 1.7 K).

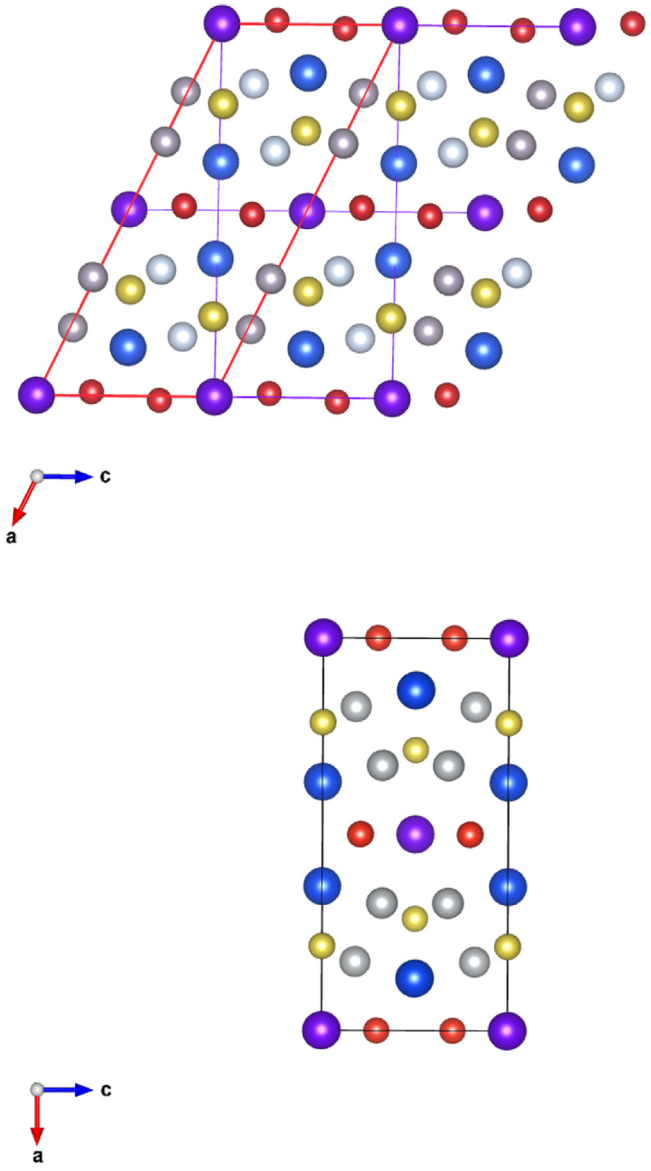

Fig. 9. Crystal structures of (top) Monoclinic and (bottom) Orthorhombic $R_3Cu_4Sn_4$, shown as projections onto the ac-plane. In the monoclinic figure, the *C2/m* cell is shown in red and the alternate *I2/m* cell is shown in blue. The R atoms are the large symbols in blue and purple. The Sn atoms are the smaller red and yellow symbols and the Cu atoms are the small grey and white-grey symbols. (For interpretation of the references to colour in this figure legend, the reader is referred to the web version of this article.)

Table 4
Crystallographic data (orthorhombic *Immm*) for $Dy_3Cu_4Sn_4$ obtained by refinement of the 1.7 K SXRD pattern.

Atom	Site	*x*	*y*	*z*
Dy	2*a*	0	0	0
Dy	4*f*	0.3669(14)	1/2	0
Cu	8*m*	0.3246(48)	0	0.3223(24)
Sn	4*e*	0.2150(22)	0	0
Sn	4*j*	1/2	0	0.2049(35)
	a (Å)	14.5710(24)		
	b (Å)	4.4246(7)		
	c (Å)	6.8924(11)		
	R (F)	9.2		
	R (Bragg)	6.0		

Finally, in Table 5 we give the lattice parameters of the $R_3Cu_4Sn_4$ compounds determined by simultaneous refinement of the X-ray and neutron powder diffraction patterns obtained in the monoclinic states. This table shows the relationship between the two descriptions of the monoclinic cell (*C2/m* and *I2/m*).

The observation that the temperature at which the crystallographic transformation occurs scales linearly with the ionic radius of the rare-earth suggests a steric/chemical mechanism for the distortion, rather than a magnetic mechanism. (The primary magnetic ordering temperatures of the four compounds studied here are 14 K (Dy), 8 K (Ho), 6 K (Er) [19] and 2.8 K (Tm) [21], all much lower than the observed structural transformation temperatures).

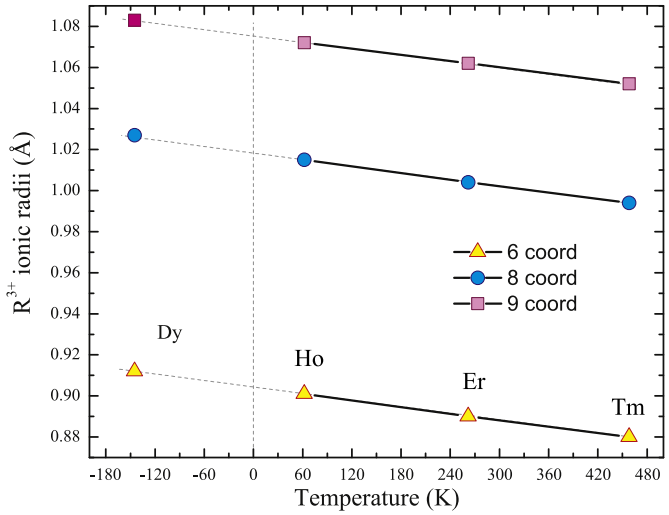

Fig. 10. Variation of the crystallographic transformation temperature with the ionic radius of the rare earth.

Table 5
Lattice parameters of the monoclinic $R_3Cu_4Sn_4$ (R = Ho, Er and Tm) phases given in the two possible crystallographic settings for the monoclinic cell. For the sake of comparison at similar temperatures we include the $Tm_3Cu_4Sn_4$ results obtained by Baran et al. at 4.9 K [21].

R	*T*(K)	Space group	*a* (Å)	*b* (Å)	*c* (Å)	*β* (°)
Ho	1.7	*I2/m*	14.5445(3)	4.4096(1)	6.8863(1)	90.26(1)
Ho	1.7	*C2/m*	16.0641(5)	4.4096(1)	6.8863(1)	115.12(1)
Er	1.7	*I2/m*	14.5003(5)	4.3929(2)	6.8810(2)	90.48(1)
Er	1.7	*C2/m*	15.9980(5)	4.3928(1)	6.8810(2)	114.99(1)
Tm	295	*I2/m*	14.4911(3)	4.3898(1)	6.8931(1)	90.54(1)
Tm	295	*C2/m*	15.9887(3)	4.3898(1)	6.8931(1)	115.0(1)
Tm [21]	4.9	*I2/m*	14.4608(31)	4.3898(8)	6.8855(16)	90.640(11)
Tm [21]	4.9	*C2/m*	16.0856(34)	4.3838(8)	6.8855(16)	115.982(14)

At this stage, it is difficult to identify the actual mechanism underlying this observation but one possibility is the dependence of the crystal structure on the valence electron concentration. In this case, the lanthanide contraction with increasing atomic number leads to an approximately linear decrease in unit cell volume and a corresponding increase in valence electron concentration. Such an effect has been identified in the magnetocaloric intermetallic compounds in the $Gd_5(Si,Ge)_4$ series [33,34]. It would be interesting to carry out synchrotron X-ray diffraction on the $R_3Cu_4Sn_4$ compounds as a function of applied pressure to follow the evolution of the crystallographic transition temperature with the changing cell volume. We are also currently exploring the use of Density Functional Theory calculations at $T = 0$ to compare the free energies of the orthorhombic and monoclinic unit cells as a function of cell volume (and, by extension, rare-earth radius).

5. Conclusions

We have investigated the orthorhombic to monoclinic structural transformation in the intermetallic compounds $R_3Cu_4Sn_4$ (R = Ho, Er, Tm). This crystallographic transformation from the *Immm* to the *C2/m* (*I2/m*) space group occurs at 62(2) K for R = Ho, 262(2) K for R = Er and 458(3) K for R = Tm [6]. No such distortion was observed for R = Dy, down to 1.7 K, consistent with the observed linear scaling between the transformation temperature and the ionic radius of the rare-earth.

Acknowledgements

JMC is grateful to the University of New South Wales (Grant SPF01) for its financial support. Initial parts of this work were carried out while JMC was on the faculty of the University of Manitoba, supported by the Canada Research Chairs programme (Grant 203392) and the Canadian funding agencies NSERC (Grants 355414-2008, 42310-2013), CFI (Grants 23406, 23285) and MRIF. DHR acknowledges support from Fonds Québécois de la Recherche sur la Nature et les Technologies. We are grateful to the staff of the LNLS synchrotron, Campinas, Brazil and the CNBC, Chalk River, Canada, for their technical and scientific support provided during the course of the diffraction measurements. Finally, we thank Robert Gagnon (McGill U.) for preparation of the $Er_3Cu_4Sn_4$ sample.

References

[1] Ryan DH, Cadogan JM, Voyer CJ, Napoletano M, Riani P, Cranswick LMD. Mod Phys Lett B 2010;24:1–28.
[2] Wawrzyńska E, Szytuła A. Mat Sci Pol 2006;24:543–9.
[3] Rieger W. Monatsh Chem 1970;101:449–62.
[4] Thirion F, Steinmetz J, Malaman B. Mat Res Bull 1983;18:1537–42.
[5] Romaka L, Romaka VV, Davydov V. Chem Met Alloys 2008;1:192–7.
[6] Muñoz Pérez S, Cobas R, Susilo RA, Cadogan JM. J Phys Conf Ser 2011;286. 012018 (5 pp).
[7] Muñoz Pérez S, Cobas R, Cadogan JM, Ryan DH, Lora-Serrano R, Figueira MJS, et al. Acta Cryst 2011;A67:C247.
[8] Singh S, Dhar SK, Manfrinetti P, Palenzona A. J Magn Magn Mater 2002;250: 190–6.
[9] Singh S, Dhar SK, Manfrinetti P, Palenzona A. J Alloys Compd 2000;298:68–72.
[10] Zaharko O, Keller L, Ritter C. J Magn Magn Mater 2002;253:130–9.
[11] Wawrzyńska E, Hernández-Velasco J, Penc B, Szytuła A. J Phys Condens Matter 2004;16:45–52.
[12] Penc B, Kaczorowski D, Szytuła A, Winiarski A, Zarzycki A. Intermetallics 2007;15:1489–96.
[13] Voyer CJ, Ryan DH, Cadogan JM. J Appl Phys 2009;105. 07D508 (3 pp).
[14] Szytuła A, Wawrzyńska E, Penc B, Stüsser N, Zygmunt A. Phys B 2003;327: 167–70.
[15] Szytuła A, Wawrzyńska E, Penc B, Stüsser N, Tomkowicz Z, Zygmunt A. J Alloys Compd 2004;367:224–9.
[16] Szytuła A, Jezierski A, Penc B, Wawrzyńska E, Zygmunt A. Phys Stat Sol 2006;243B:299–303.
[17] Voyer CJ, Ryan DH, Napoletano M, Riani P. J Phys Condens Matter 2007;19. 156209 (10 pp).
[18] Łatka K, Pacyna AW, Pöttgen R, Schappacher FM. Acta Phys Pol 2008;114A: 1501–8.
[19] Wawrzyńska E, Hernández-Velasco J, Penc B, Sikora W, Szytuła A, Zygmunt A. J Phys Condens Matter 2003;15:5279–96.
[20] Szytuła A, Penc B, Zarzycki A. J Phys Conf Ser 2010;200. 032072 (5pp).
[21] Baran S, Kaczorowski D, Szytuła A, Gil A, Hoser A. J Phys Condens Matter 2013;25. 066012 (9pp).
[22] Gondek Ł, Szytuła A, Kaczorowski D, Szewczyk A, Gutowska M, Prokhnenko O. Intermetallics 2007;15:583–92.
[23] Gondek Ł, Arulray A, Baran S, Nenkov K, Penc B, Szytuła A, et al. J Phys Condens Matter 2008;20. 295205 (6pp).
[24] Gondek Ł, Szytuła A, Prokhnenko O. Acta Phys Pol 2008;113A:1179–84.
[25] Ryan DH, Cadogan JM, Gagnon R, Swainson IP. J Phys Condens Matter 2004;16:3183–98.
[26] Zaharko O, Keller L. Experimental report. Paul Scherrer Institute; 2001 [in press].
[27] Rodríguez-Carvajal J. Physica B 1993;192:55–69.
[28] Roisnel T, Rodríguez-Carvajal J. Mater Sci Forum 2001;378–81:118–23.
[29] Bilbao Crystallographic Server, http://www.cryst.ehu.es.
[30] Momma K, Izumi F. VESTA 3 for three-dimensional visualization of crystal, volumetric and morphology data. J Appl Cryst 2011;44:1272–6.
[31] Krause W, Nolze G. J Appl Cryst 1996;29:301–3.
[32] Shannon RD. Acta Cryst A 1976;32:751–67. Jia YQ. J. Solid State Chem. 1991;95:184–7.
[33] Choe W, Pecharsky VK, Pecharsky AO, Gschneidner Jr KA, Young VG, Miller GJ. Phys Rev Lett 2000;84:4617–20.
[34] Ryan DH, Lee-Hone NR, Cadogan JM, Ahn K, Pecharsky VK, Gschneidner Jr KA. Hyp Int 2012;208:59–63.